JOURNAL OF SOLID STATE CHEMISTRY 80, 235–240 (1989)

Solid Solutions and Phase Transitions in Langbeinites (I): $M_2^+Mn_2(SO_4)_3$ (M^+ = K, NH_4, Tl)

M. L. MARTINEZ SARRIÓN,* A. RODRÍQUEZ CLEMENTE, AND L. MESTRES VILA

Facultad de Química, Departamento de Química Inorgánica, Diagonal 647, 08028 Barcelona, Spain

Received October 4, 1988; in revised form January 27, 1989

Solid solutions of general formula $K_x(NH_4)_{2-x}Mn_2(SO_4)_3$ ($0 < x < 2$) and $K_yTl_{2-y}Mn_2(SO_4)_3$ ($0 < y < 2$) have been prepared. All of the phases within the composition range studied have been established, and their cubic symmetry at room temperature has been confirmed. The cell parameters for each member of the solid solutions have been determined. The substitution has been found to be homogeneous. Differential scanning calorimetry experiments of solid solution with $x = 2.00$, 1.81, and 1.49, and $y = 2.00$ and 1.79 have been carried out in order to study the transition mechanism in the ferroelastic langbeinite $K_2Mn_2(SO_4)_3$. The T_c for the phase transition $P2_13$–$P2_12_12_1$ is −75.9°C. The mixed crystals of NH_4^+ show phase transition up to 10% substitution, with a decrease in both T_c and ΔH. On the other hand, the phase transition disappears in the mixed crystals of Tl^+. The size of the M^+ ion plays an important role in the phase transition.

Introduction

Recently, the langbeinite crystals, $M_2^+M_2^{2+}(SO_4)_3$, have attracted much attention, as some of them show ferroelectric and ferroelastic phase transitions (*1–4*).

The prototype of langbeinites is mineral $K_2Mg_2(SO_4)_3$. The structure of this compound has been determined by Zemann and Zemann (*5*). The double sulfate salts of langbeinites are cubic with space group $P2_13$.

Hikita classified the phase transitions in langbeinites into two groups. Group I represented by the prototype $Tl_2Cd_2(SO_4)_3$ has the transition scheme $P2_13$–$P2_1$–$P1$–$P2_12_12_1$ corresponding to paraelectric/elastic–ferroelectric–ferroelectric–ferroelastic transitions (*6*). Group II has the transition scheme $P2_13$–$P2_12_12_1$ (paraelastic–ferroelastic transition). The prototype is $K_2Mn_2(SO_4)_3$ (KMS), with a cubic–orthorhombic transition at −82°C (*2*). Langbeinites without any transitions at atmospheric pressures belong to group III. $K_2Mg_2(SO_4)_3$ and examined $(NH_4)_2Mn_2(SO_4)_3$, (AMS) and $Tl_2Mn_2(SO_4)_3$ (TMS) belong to this class (*7*).

The phase transition mechanisms of these crystals are far from clear despite detailed dielectric, optical, and elastic measurements available (*8–11*). In the langbeinite $K_2Cd_2(SO_4)_3$, X-ray structural studies revealed that the SO_4^{2-} ions rotate slowly with temperature (*12*). Yamada *et al.* (*13*) suggest that in the cubic phase there are two statistically equivalent positions for each oxygen atom. In the ordered

0022-4596/89 $3.00

orthorhombic phase, one of the equivalent positions is chosen along with a small displacement of the SO_4^{2-} ion.

Kreske and Devarajan (*3*) studied the phase transitions in $K_2Mn_2(SO_4)_3$ by means of vibrational spectroscopy. This group of crystals, if characterized by displacive type of phase transition, should show the presence of soft modes in the Raman spectra in both cubic and orthorhombic phases. The evidence for the phase transition is clearly seen in the splitting of the SO_4^{2-} internal vibration Raman bands in the cubic and orthorhombic phases. For a possible mechanism of the phase transition an order–disorder mechanism can be considered which is associated with the ordering of the SO_4^{2-} ions; but there are different possible types of ordering.

More recently, Speer and Salje (*4*) asserted that, whereas the SO_4^{2-} tetrahedra in these compounds are almost undistorted, the two symmetry-independent coordination polyhedra of M^{2+} are highly distorted octahedra with trigonal site symmetry $P2_13$. The deformation of the oxygen octahedra and the off centering of M^{2+} along the trigonal axis show systematic dependencies on the ionic radii and the electronegativities of the M^{2+} ions, indicating different M^{2+}–O bonding.

The octahedral deformations show also linear correlations with the phase transition temperatures ($P2_13$–$P2_12_12_1$) of the different compounds. This observation leads to a model for the phase transition mechanism which is based on thermal instabilities of the M^{2+}–O and M^{+}–O polyhedral distortions. The cubic, high-temperature phase is characterized by high symmetric oxygen coordinations around M^{2+} which show increasing distortion with decreasing temperature.

By studying the formation of solid solutions (replacing the metal M^+ in langbeinite showing phase transition) we wish to contribute to the knowledge of the mechanism by which the corresponding transition occurs.

Experimental

The systems investigated are $K_x(NH_4)_{2-x}Mn_2(SO_4)_3$ (KAMS) and $K_yTl_{2-y}Mn_2(SO_4)_3$ (KTMS) over the composition ranges $2.00 > x > 0$ and $2.00 > y > 0$.

The starting langbeinites KMS, AMS, and TMS, were obtained by evaporation of the 1 : 2 molar ratio aqueous solution of analytical-grade K_2SO_4–$MnSO_4 \cdot H_2O$, $(NH_4)_2SO_4$–$MnSO_4 \cdot H_2O$, and Tl_2SO_4–$MnSO_4 \cdot H_2O$, at 120°C (*14*) (thermostated bath with ethyleneglycol).

The mixed crystals of general formula KAMS and KTMS were obtained mixing aqueous solution of the langbeinites KMS–AMS and KMS–TMS in varying proportions.

The cubic symmetry at room temperature for these crystals was confirmed by X-ray powder diffraction. The samples were mounted on a Siemens automatic diffractometer, D500-DACOMP. Ni-filtered, Cu$K\alpha$ radiation was used with a scan speed equal to $\frac{1}{2}\theta$ min^{-1} and a θ range of 5–30°.

The indexation was carried out from the values of $K_2Mn_2(SO_4)_3$ (PDF 20-209). Cell parameters for each phase were refined by a full-matrix least-squares method from the cell parameters of $K_2Mn_2(SO_4)_3$. The computer program used was AFFMAIL (*15*). Atomic absorption analyses were carried out on a spectrophotometer PYE UNICAM S.P. 1900. Elemental analyses were carried out in a Perkin–Elmer 240 microanalyzer. The infrared spectra were recorded on a Perkin–Elmer 1330 spectrophotometer; samples prepared as KBr pellets or Nujol mulls gave the same spectra. The heat flows of the samples were measured with a Perkin–Elmer differencial scanning calorimetric DSC 7 in the temperature range +30 to −170°C and at a rate of 10.0°C/min. The

TABLE I

ANALYSES OF SOLID SOLUTIONS $K_x(NH_4)_{2-x}Mn_2(SO_4)_3$

	% K	% NH_4
KMS	16.39	—
KAMS-1	14.97	0.64
KAMS-2	14.32	0.95
KAMS-3	12.53	1.81
KAMS-4	9.90	3.18
KAMS-5	7.70	4.26
KAMS-6	6.19	5.05
KAMS-7	3.10	6.61
AMS	—	8.30

TABLE III

COMPOSITION OF MIXED CRYSTALS $K_x(NH_4)_{2-x}Mn_2(SO_4)_3$

KMS	$K_2Mn_2(SO_4)_3$
KAMS-1	$K_{1.81}(NH_4)_{0.17}Mn_2(SO_4)_3$
KAMS-2	$K_{1.72}(NH_4)_{0.25}Mn_2(SO_4)_3$
KAMS-3	$K_{1.49}(NH_4)_{0.47}Mn_2(SO_4)_3$
KAMS-4	$K_{1.16}(NH_4)_{0.81}Mn_2(SO_4)_3$
KAMS-5	$K_{0.89}(NH_4)_{1.08}Mn_2(SO_4)_3$
KAMS-6	$K_{0.71}(NH_4)_{1.26}Mn_2(SO_4)_3$
KAMS-7	$K_{0.35}(NH_4)_{1.62}Mn_2(SO_4)_3$
AMS	$(NH_4)_2Mn_2(SO_4)_3$

measurements were made on polycrystalline samples.

Results

The results of the solid solution analyses are given in Tables I and II. The composition of the different phases has been established by chemical analyses. The results are given in Tables III and IV. The results of X-ray diffraction are shown in Tables V and VI.

The IR absorption spectra clearly show the internal vibrational modes (ν_1, ν_2, ν_3, and ν_4) of the tetrahedral SO_4 group in all of the crystals: ν_1 above 1000 cm^{-1}, ν_2 at 470 cm^{-1}, ν_3 between 1170 and 1080 cm^{-1}, and ν_4 between 640 and 605 cm^{-1}. All samples with NH_4^+ show ν_3 and ν_4 vibrations in the region 1410–3200 cm^{-1}.

Figure 1 shows the heat flow (mW)/temperature (°C) of $K_2Mn_2(SO_4)_3$ (sample weight = 56.430 mg; T_c = −75.9°C; ΔH = 1.626 J/g). Figure 2 shows the heat flow (mW)/temperature (°C) of $K_{1.81}(NH_4)_{0.17}Mn_2(SO_4)_3$ (sample weight = 54.070 mg; T_c = −110.9°C; ΔH = 0.235 J/g). Figure 3 shows the heat flow (mW)/temperature (°C) of $K_{1.49}(NH_4)_{0.47}Mn_2(SO_4)_3$. Figure 4 shows the heat flow (mw)/temperature (°C) of $K_{1.79}Tl_{0.19}Mn_2(SO_4)_3$. A small hump occurred reproducibly in all the DSC experiments at ca. −48°C. Sample dependence of this small anomaly is yet to be studied. The Rb

TABLE II

ANALYSES OF SOLID SOLUTIONS $K_yTl_{2-y}Mn_2(SO_4)_3$

	% K	% Tl
KMS	16.39	—
KTMS-1	13.81	7.66
KTMS-2	10.64	15.92
KTMS-3	8.66	20.62
KTMS-4	6.59	26.76
KTMS-5	5.15	29.90
KTMS-6	3.38	35.25
KTMS-7	1.78	40.11
TMS	—	50.67

TABLE IV

COMPOSITION OF MIXED CRYSTALS $K_yTl_{2-y}Mn_2(SO_4)_3$

KMS	$K_2Mn_2(SO_4)_3$
KTMS-1	$K_{1.79}Tl_{0.19}Mn_2(SO_4)_3$
KTMS-2	$K_{1.47}Tl_{0.51}Mn_2(SO_4)_3$
KTMS-3	$K_{1.27}Tl_{0.70}Mn_2(SO_4)_3$
KTMS-4	$K_{1.02}Tl_{0.96}Mn_2(SO_4)_3$
KTMS-5	$K_{0.84}Tl_{1.13}Mn_2(SO_4)_3$
KTMS-6	$K_{0.58}Tl_{1.40}Mn_2(SO_4)_3$
KTMS-7	$K_{0.30}Tl_{1.67}Mn_2(SO_4)_3$
TMS	$Tl_2Mn_2(SO_4)_3$

TABLE V

CELL PARAMETERS AND VOLUME FOR EACH MEMBER OF THE SOLID SOLUTION $K_x(NH_4)_{2-x}Mn_2(SO_4)_3$

	a (Å)	V (Å^3)	ε	NP
KMS	10.1194(9)	1036.2(3)	1.07	26
KAMS-1	10.125(1)	1037.9(3)	1.79	26
KAMS-2	10.130(1)	1039.6(3)	1.23	25
KAMS-3	10.137(2)	1041.7(6)	1.87	26
KAMS-4	10.151(1)	1046.1(3)	1.50	25
KAMS-5	10.163(2)	1049.8(6)	2.03	24
KAMS-6	10.169(1)	1051.6(3)	1.41	27
KAMS-7	10.182(1)	1055.6(3)	1.24	28
AMS	10.1908(6)	1058.3(2)	0.71	26

Note. NP, number of peaks used in the cell parameter determination.

H_2PO_4 and $(NH_4)_{0.89}Rb_{0.11}H_2PO_4$ showed similar small humps at ca. −148 and −175°C, respectively (*16*).

Discussion

The X-ray diffraction patterns of the samples indicated only reflections attributable to the pure phases. In order to determine the homogeneity of the substitution between the K^+ and NH_4^+ or K^+ and Tl^+ ions, a linear regression of cell parameters and cell volume has been carried out. The largest deviations from linearity are within three times the highest standard deviation,

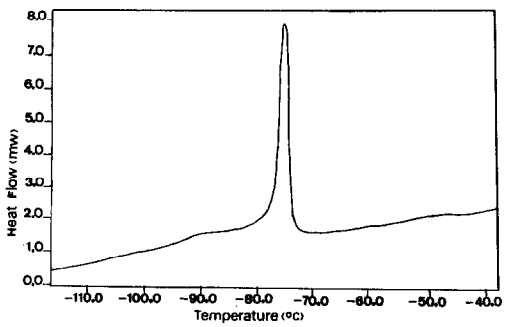

FIG. 1. Heat flow of $K_2Mn_2(SO_4)_3$.

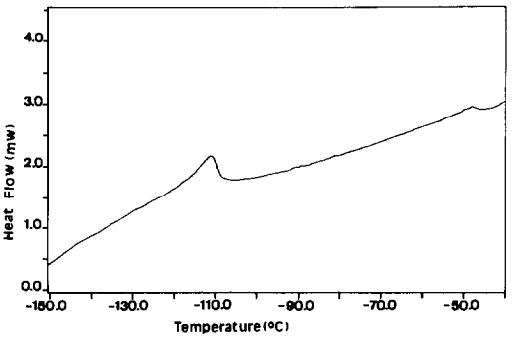

FIG. 2. Heat flow of $K_{1.81}(NH_4)_{0.17}Mn_2(SO_4)_3$.

to assume the substitution to be homogeneous.

The infrared spectra are typical of the SO_4^{2-} ion, and the selection rules for C_1 symmetry, approximately adhered to ν_1 and ν_2 regions (symmetric vibrations), are relatively weak; ν_2 invariably appears as only one component. The stronger absorption in the ν_3 and ν_4 (asymmetric vibrations) regions and the fact that they are triply degenerate agrees with the symmetry decrease of the SO_4^{2-} groups in the langbeinites.

The atomic arrangement proposed by Zemann and Zemann (*5*) implies the SO_4 groups to be practically ideal tetrahedra in

TABLE VI

CELL PARAMETERS AND VOLUME FOR EACH MEMBER OF THE SOLID SOLUTION $K_yTl_{2-y}Mn_2(SO_4)_3$

	a (Å)	V (Å^3)	ε	NP
KMS	10.1194(9)	1036.2(3)	1.07	26
KTMS-1	10.136(1)	1041.4(3)	1.33	24
KTMS-2	10.145(1)	1044.1(3)	1.40	25
KTMS-3	10.163(1)	1049.7(3)	1.27	27
KTMS-4	10.175(1)	1053.3(3)	1.82	29
KTMS-5	10.182(1)	1055.7(3)	1.40	28
KTMS-6	10.199(1)	1060.9(3)	1.28	29
KTMS-7	10.2065(9)	1063.2(3)	1.09	29
TMS	10.2236(7)	1068.7(2)	0.81	29

Note. NP, number of peaks used in the cell parameter determination.

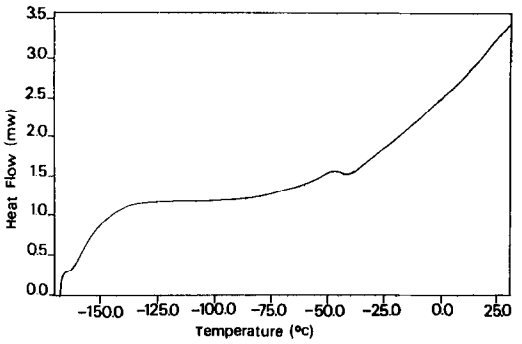

FIG. 3. Heat flow of $K_{1.49}(NH_4)_{0.47}Mn_2(SO_4)_3$.

$K_2Mg_2(SO_4)_3$, which is isostructural with $K_2Mn_2(SO_4)_3$. This observation was confirmed by Speer and Salje (*4*). Distorted coordination polyhedra occur around the metal positions. The potassium atoms have 9 nearest oxygen neighbors in the cubic phase. In the orthorhombic phase there are 10 nearest neighbors for K(1) and 9 for K(2), which is similar to the orthorhombic crystal structure of $K_2Cd_2(SO_4)_3$.

The divalent metals are always coordinated by six oxygen atoms forming a distorted octahedron. The M^{2+} position is not at the midpoint between the two oxygen triangles around the trigonal axis. With increasing ionic radius, the octahedral central position M^{2+} is pushed from the octahedra midpoint toward one triangle of oxygen atoms. Salje shows that there is a linear correlation between the octahedral deformation and the ionic radius of M^{2+}.

In the $P2_13$–$P2_12_12_1$ phase transition, there is a correlation between the critical temperature and the octahedral distortions. The structural phase transition between the cubic phase and the orthorhombic phase reduces the symmetry of the M^{2+}–O octahedra by destroying the trigonal axis. When the octahedron becomes sufficiently distorted the structural phase transition takes place.

At temperatures below T_c, the deformation of the rotation parameter, the distance between the M^{2+} position and the geometrical midpoint of the octahedra, and the relative shrinking of one triangle face with respect to a second triangle face transform according to the orthorhombic symmetry.

At temperatures far above T_c, the octahedra $M^{2+}O_6$ are highly symmetric; this high symmetry coordination is only possible at the expense of larger M^+–O distances and a rather poor packing around M^+. With decreasing temperatures, the coordination of M^{2+} becomes less symmetric, and the structural phase transition is expected to take place. In the orthorhombic phase, the MO_6 octahedra are heavily distorted, the average M^{2+}–O distances become larger, and the M^+–O distances become shorter. Therefore, the M^+O polyhedra show a closer packing at the expense of a wider MO_6 packing.

The SO_4 tetrahedra shift and rotate during the phase transition to achieve the better packing of the M^+–O polyhedron.

The mechanism by which the phase transition occurs can be explained as a result of a cooperative effect. The SO_4^{2-} tetrahedra shift and rotate, causing a decrease in the M^+–O distance, thereby making possible the distortion of the $M^{2+}O_6$ octahedra. These three factors contribute to the phase transition.

For the langbeinites containing SO_4^{2-}, Mn as the bivalent cation, and K^+, NH_4^+, or Tl^+

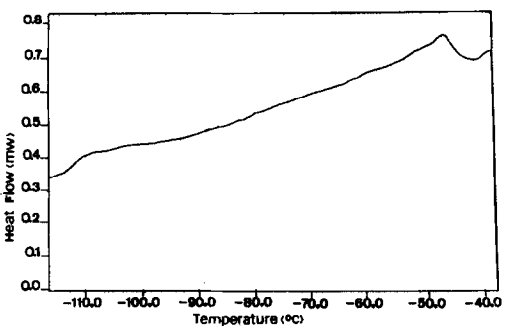

FIG. 4. Heat flow of $K_{1.79}Tl_{0.19}Mn_2(SO_4)_3$.

as the monovalent cation, the increase of the M^+ radius complicates the packing of the MnO_6 octahedra in such a way that either the transition does not take place or it takes place at a temperature too low to be detected by our equipment.

A critical size for M^{2+} should exist below which the transition does not occur, since an increase in the M^{2+} size favors the transition. In fact for $M^{2+} = Mn^{2+}$ the transition is only observed when M^+ is potassium, but for $M^{2+} = Cd^{2+}$ the langbeinites of Tl, Rb, NH_4, and K do show transition (*7*).

For the langbeinite $K_2Mn_2(SO_4)_3$, the size of the potassium ion allows the operation of the cooperative mechanism and the occurrence of the phase transition. If the substitution of NH_4^+ for K^+ is less than ca. 10%, there is still transition; however, there is a decrease in both T_c and ΔH.

The limit of substitution of K^+ by Tl^+ is less than 10% (agreeing with the larger radius of Tl^+). No phase transition is detected even at the lowest Tl^+ concentration. In fact, the only thallium langbeinite showing transition is that for which the bivalent metal is cadmium. The size of M^+ is offset by the size increase of M^{2+}, in agreement with the mechanism proposed. We can assume that real ferroelastic crystals of $Tl_2Cd_2(SO_4)_3$ as well as $K_2Mn_2(SO_4)_3$ are made up of ferroelastic domains. It is known (*6*) that three different orientations of those domains exist. Application of a mechanical field could cause favorably oriented domains to grow at the expense of the disadvantageously oriented domains. The presence of M^+–O polyhedra other than K^+–O polyhedra probably complicates the domain ordering. The existence of NH_4^+–O or Tl^+–O polyhedra replacing K^+–O polyhedra precludes a better packing and the distortion of the MnO_6 octahedrons, as well as the decrease of symmetry accompanying the phase transition to the orthorhombic phase.

Acknowledgments

The authors thank Professor E. H. Bocanegra for carrying out the thermal measurement. This work has been partially financed by "Proyecto CICYT No. PR 84-0120."

References

1. T. Hikita, S. Sato, H. Sekiguchi, and T. Ikeda, *J. Phys. Soc. Japan* **42,** 1656 (1977).
2. T. Hikita, M. Kitabatake, and T. Ikeda, *J. Phys. Soc. Japan* **49,** 1421 (1980).
3. S. Kreske and V. Devarajan, *J. Phys. C: Solid. State Phys.* **15,** 7333 (1982).
4. D. Speer and E. Salje, *Phys. Chem. Miner.* **13,** 17 (1986).
5. A. Zemann and J. Zemann, *Acta Crystallogr.* **10,** 409 (1957).
6. B. Březina and M. Glogarová, *Phys. Status Solidi A* **22,** K69 (1979).
7. T. Hikita, H. Sekiguchi, and T. Ikeda, *J. Phys. Soc. Japan* **42,** 1327 (1977).
8. M. Glogarova, *Phys. Status Solidi A* **22,** K69 (1974).
9. T. Ikeda and G. Yasuda, *Japan. J. Appl. Phys.* **14,** 1287 (1975).
10. N. Yamada, Y. Chubachi, and T. Ikeda, *J. Phys. Soc. Japan* **45,** 1638 (1978).
11. M. Maeda, *J. Phys. Soc. Japan* **47,** 1581 (1979).
12. S. C. Abrahams, F. Lissalde, and J. L. Bernstein, *J. Chem. Phys.* **68,** 1926 (1978).
13. N. Yamada, M. Maeda, and M. Adachi, *J. Phys. Soc. Japan* **50,** 907 (1981).
14. G. Gatow and J. Zeeman, *Z. Anorg. Allg. Chem.* **293,** 233 (1958).
15. J. Stewart, "AFFMAIL: A Computer Program for Cell-Parameters Refinement." University of Bourdeaux (1970).
16. K. Moriya, T. Matsuo, and M. Suga, *Japan. J. Appl. Phys.* **24**(Suppl. 24-2), 955 (1985).